Morteza Mollazadeh, Ashraf Fakhari*, Tohid Mortezazadeh, Farshid Babapour Mofrad and Ali Jamali Nazarie

Synthesis, MTT assay, 99m-Technetium radiolabeling, biodistribution evaluation of radiotracer and *in vitro* magnetic resonance imaging study of P,N-doped graphene quantum dots as a new multipurpose imaging nano-agent

https://doi.org/10.1515/ract-2023-0180
Received June 6, 2023; accepted March 14, 2024;
published online May 24, 2024

Abstract: In this study, a new nano-structure, N,P-doped graphene quantum dots (N,P-GQDs), were synthesized as multipurpose imaging agent for performing scintigraphy and magnetic resonance imaging (MRI). Some standard characterization methods were used to identify the nano-structure. *In vitro* cytotoxicity evaluation using MTT assay revealed that N,P-GQDs nanoparticles had no significant cytotoxicity after 24 and 48 h against normal (MCF-10A) and cancerous (MCF 7) human breast cell line in concentration up to 200 µg/mL. The N,P-GQDs were radiolabeled with Technetium-99m as ^{99m}Tc-(N,P-GQDs) and the radiochemical purity was assayed by ITLC concluding RCP ≥ 95 %. The passing of ^{99m}Tc-(N,P-GQDs) through 0.1 µm filter demonstrated that 70.8 % of particles were <0.1 µm. In order to perform scintigraphy, the ^{99m}Tc-(N,P-GQDs) were injected to female healthy Wistar rats. The results showed that the radio-complex was captured and eliminated just by kidneys. Moreover, *in vitro* T_1-weighted phantom MRI imaging showed that the N,P-GQDs have proper relaxivity in comparison to Dotarem® as a clinically available contrast agent. The results showed that the N,P-GQDs have potential to be considered as a novel and encouraging agent for both molecular MRI and nuclear medicine imagings.

Keywords: radiolabeling; graphene quantum dots; technetium-99m; biodistribution

1 Introduction

Over the last few years, many types of nanoparticles (NPs) have been used in different fields of sciences, as well as modern-day medicine. NPs are defined as particles in size of <100 nm, so, a wide range of natural and synthetic molecules could be considered as NPs [1]. Graphene quantum dots (GQDs), as synthetic types of NPs are widely used in a variety of fields because of their individual characteristics. These NPs are prepared as layered structures (dots) with ≥2–10 layers in size <100 nm diameter with especial characteristics, including photoluminescence (PL) properties, as well as thermal and electrical conductivity [2]. In addition, biocompatibility, economic way of preparation and low cytotoxicity made them as an interesting NPs in the fields of bio-imaging, pharmacy, photothermal and photodynamic therapy of cancerous cells [3–6].

The synthesis of GQDs derivatives with desirable photoluminescence emission leads them to be considered as bio-imaging agents [3]. The layered structure and possibility of 200 % loading can result in the preparation of efficient drug delivery systems (DDS) based on GQDs [7, 8]. There are some promising studies that show the GQDs used in anti-cancer agents increase drug efficacy in addition to delivery. Moreover, these assemblies could be used for assaying drug accumulation rate and imaging [9–11]. Generally, fluorescence imaging encounters problems such as absorbance, dispersion and auto-fluorescence that cause disruption of rays [12, 13].

In order to improve imaging quality, the radiolabeling potential of GQDs with gamma emitting radioisotopes has

***Corresponding author: Ashraf Fakhari**, Medical Radiation Sciences Research Team, Tabriz University of Medical Sciences, Tabriz, Iran, E-mail: Fakhari.a@tbzmed.ac.ir. https://orcid.org/0000-0002-1732-5544
Morteza Mollazadeh and Farshid Babapour Mofrad, Department of Medical Radiation Engineering, Science and Research Branch, Islamic Azad University, Tehran, Iran, E-mail: mortaza.mollazadeh@iau.ac.ir (M. Mollazadeh), babapour@srbiau.ac.ir (F.B. Mofrad)
Tohid Mortezazadeh, Department of Medical Physics, Faculty of Medicine, Tabriz University of Medical Sciences, Tabriz, Iran, E-mail: tmortezazadeh@tbzmed.ac.ir
Ali Jamali Nazarie, Department of Engineering, Shahrood Branch, Islamic Azad University, Shahrood, Iran, E-mail: jamali@iau-shahrood.ac.ir

recently been introduced [14]. These assemblies can be used multi-purposely for different applications and imaging simultaneously. Technetium-99m with half-life of 6 h and gamma energy of 140 keV is a common gamma emitting radioisotope in diagnostic nuclear medicine. Also, availability by ^{99}Mo/^{99m}Tc generator makes that more interesting for preparing diagnostic radio-agents [15].

Magnetic resonance imaging (MRI) is known as a potent, noninvasive and sensitive clinical imaging modality due to its capacity to produce precise three-dimensional anatomical images with high spatial resolution and virtually unlimited tissue penetration depth [16]. If needed, patients are injected by contrast agent prior to undergoing MRI in order to improve the visibility of organs in this imaging. The most popular MRI contrast agents are based on the metal gadolinium; however, these metal compounds may be dangerous for young children or patients with kidney disorders. Although, metal-based contrast agents (CAs) in mesoporous nanocarriers modify metal release to lessen toxicity, the future degradation may still release metal to the environment causing adverse effects on the body [17]. A safety warning about the potential long-term deposition of Gd-based contrast agents in the brain tissue was also recently reported by the Food and Drug Administration (FDA) [18]. Therefore, there is an urgent need to create nonmetal MRI contrast agents with better sensitivity and functionality than common T_1 contrast agents. This has prompted the creation of numerous types of organic metal-free CAs for MRI [19, 20]. In this study, we developed metal-free phosphor/nitrogen-doped graphene quantum dots (N,P-doped-GQDs) NPs as a potent imaging agent for both MRI (with safe T_1 contrast) and nuclear medicine imaging (Figure 1).

When using contrast agents based on graphene (graphene dots doped with heteroatoms), the carbon bonds with heteroatoms act as magnetic centers and magnetic dipoles. Also, they can interact with water molecules and cause a change in the spin relaxation time of hydrogen atoms in the region where the contrast material is present. They amplify the resulting signal to improve MRI [21, 22]. During the synthesis of GQDs, it was tried to synthesize the samples in such a way that the interaction of water molecules with NPs is provided [23]. The magnetic property is probably produced by introducing both vacancies and elemental P-doped molecules as the substitutional defect. Like that, metal-free graphite and graphene oxide could also produce paramagnetism by introducing dipolar C–F bonds [24, 25], but in comparison to them, the GQDs are considered as agent with lower toxicity. So, the prepared nano-structure could be applied as a metal-free MRI contrast agent. Furthermore, the N,P-GQDs were radiolabeled with Technetium-99m as ^{99m}Tc-(N,P-GQDs) to prepare multi-purpose imaging agent. These assemblies could be loaded with agents, targeted and radiolabeled with Technetium-99m simultaneously for selective assay. Based on radiolabeling, it is suggested that the ^{99m}Tc-(P,N-GQDs) be used in targeting drug delivery for assaying concentration of agent in target through scintigraphy. Also, this structure could be used for indirect radiolabeling of agents without any potential for radiolabeling, through conjugation of agent-P,N-GQDs assemblies. This study suggests the N,P-GQDs as a dual imaging agent for MRI and scintigraphy, highlighting their potential to address or alleviate some challenges associated with these imaging methods.

2 Materials and methods

During this investigation, N,P-GQDs were synthesized by microwave [22]. Technetium-99m was eluted from ^{99}Mo/^{99m}Tc generator as sodium ^{99m}Tc-pertechnetate ($^{99m}TcO_4^-Na^+$). The generator was purchased from

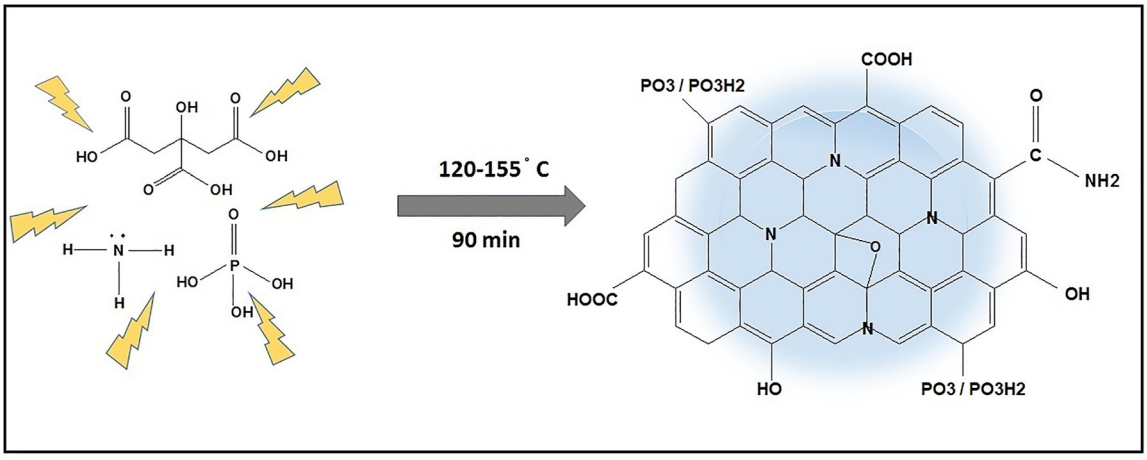

Figure 1: Schematic production route to N,P-GQDs. Because the phosphate group is a weak acid, the PO_3 groups in the product should be either PO_3H_2 or PO_3^{2-}.

Pars Isotope Co. Stannous chloride dihydrate was obtained from Sigma-Aldrich Co. Chromatography paper Silica gel (SG) 60 F254, sodium acetate, acetic acid glacial, phosphoric acid, acide L(+)-ascorbico (ascorbic acid), ammonia solution 25 %, phosphoric acid and solvents were obtained from the Merck Co. Millipore filters at 0.1 µm (Minisart® High Flow with polyethersulfone (PES) with a pore size of 0.1 µm) were purchased from Sartorius Co. Female Wistar rats were provided by the Animal Studies Center of Tabriz University of Medical Sciences, Iran. Gd-DOTA (Dotarem®) was obtained from Bayer Health Care Pharmaceuticals Inc. (Montville, NJ, USA). Also, this study was performed in strict accordance with the NIH guidelines for the care and use of laboratory animals (NIH Publication No. 85-23 Rev. 1985). The study was approved by the Medical Radiation Sciences Research Team and Research Ethics Committee (REC) of Tabriz University of Medical Sciences, Iran.

2.1 Synthesis and characterization of N,P-GQDs

We mixed 15 mg of citric acid monohydrate, 3 mL of ammonia solution 25 %, 1 mg of phosphoric acid (=0.53 mL), and three drops of distilled water in the Microsynth microwave's cell. The Microsynth was programmed to raise the temperature as t_0 = 120 °C to t_{2h} = 155 °C (rate of 0.38 °C min^{-1} under a constant power of 1000 W) step by step. Then, the mixture of reactor was washed in ethanol twice for purification of N,P-GQDs. The N,P-GQDs precipitate was filtered from ethanol and dried in oven at 80 °C for 72 h and studied by chemical characterization methods including TGA (by LINSEIS ThERMAL Balance L81/1750), TEM (by FP-6200 spectrofluorometer, (JASCO Corporation, Tokyo, Japan), FT-IR (with KBr by a Perkin-Elmer FT-IR spectrometer), XRD (by Bruker AXS model D8 Advance), and XPS (by ESCALAB 250. Xi from Thermo Scientific using Mg X-ray resource) [14].

2.2 Preparation of acetate buffer (pH = 5.5)

We mixed 0.73 g of NaOAc (sodium acetate) with 590 µL of HOAc (acetic acid glacial 100 %), and diluted it to 100 mL, then pH was adjusted to pH 6.0–6.3.

2.3 Preparation of stannous chloride solution

In order to prepare stock solution of stannous chloride, 3 mg of stannous chloride dihydrate ($SnCl_2{\cdot}2H_2O$) was dissolved in 3 mL of degassed (bubbled with nitrogen gas) HCl 0.1 N (1 mg $SnCl_2{\cdot}2H_2O$/1 mL HCl 0.1 N) and vacuumed to prevent deterioration of $SnCl_2{\cdot}2H_2O$.

2.4 Preparation of ascorbic acid solution

40 mg of L(+)-ascorbic acid was dissolved in 1 mL distilled water (40 mg L(+)-ascorbic acid/1 mL water) for preparation of ascorbic acid solution and then bubbled under nitrogen gas.

2.5 Radiolabeling of N,P-GQDs with Technetium-99m as ^{99m}Tc-(N,P-GQDs)

To this end, 15 mg of N,P-GQDs were dispersed in 0.5 mL of distilled water and 0.5 mL of acetate buffer (1:1). Then 300 µL of NaOH 0.1 M was added to the dispersion for fixing pH at 5.5–6.5. The dispersion was bubbled under nitrogen gas to prevent oxidation of $SnCl_2{\cdot}2H_2O$. After that, 37 MBq of $^{99m}TcO_4^-$ solution milked from ^{99}Mo/^{99m}Tc generator was added to N,P-GQDs dispersion. Then, 100 µL of prepared stannous chloride solution and 100 µL of prepared L(+)-ascorbic acid solution were added to the mixture of reaction and the vial (located in lead shield) was heated to 95 °C and stirred at 500 RPM respectively for 40 min. The effect of involved variables including pH, temperature, amount of N,P-GQDs and reductant were studied to improve radiolabeling quality. The radiochemical purity (RCP) was assayed through instant thin layer chromatography (ITLC). The radiotracer was prepared at RCP ≥ 95 %. The calculated RCP was ≥96 %.

2.6 The radiochemical purity (RCP%) assessments

The routine instant thin layer chromatography (ITLC) method was used to calculate RCP% of radiolabeling reaction. Two systems of chromatography with SG (as instant phase) and different solvents, including acetone and mixture (mixture of H_2O: EtOH: ammonia solution 25 % (5:2:1 v/v)) were separately applied. The strips of SG (1 cm × 10 cm) were spotted by reaction mixture and placed in two distinct chromatography tanks with different solvents. The separation of radio-ingredients consisting free $^{99m}TcO_4^-$, colloid ($^{99m}TcO_2$: reduced hydrolyzed technetium) and ^{99m}Tc-(N, P-GQDs) were shown in Table 1. After performing the chromatography, the strips were removed from the tanks and cut in 1 cm pieces. The pieces were counted in a time settled well counter (Biodex Medical System, UPTAKE STAND 200 CTYSTAL, model 187–220, No. 120397604 equipped with a well counter) for assaying count per minute (CPM). Percentage of the $^{99m}TcO_2$, free $^{99m}TcO_4^-$ and ^{99m}Tc-(N,P-GQDs) were calculated by Equations (1)–(3).

$$\%^{99m}TcO_4^- = \frac{Cpm\left(^{99m}TcO_4^-\right)}{Cpm\left[^{99m}TcO_4^- + {}^{99m}TcO_2 + {}^{99m}Tc - (N.P - GQDs)\right.} \quad (1)$$

$$\%^{99m}TcO_2 = \frac{Cpm\left(^{99m}TcO_2\right)}{Cpm\left[^{99m}TcO_4^- + {}^{99m}TcO_2 + {}^{99m}Tc - (N.P - GQDs)\right.} \quad (2)$$

$$\%RCP \text{ of } {}^{99m}Tc - (N.P - GQDs) = 100 - \%\left[^{99m}TcO_4^- + {}^{99m}TcO_2\right] \quad (3)$$

2.7 Serum stability of ^{99m}Tc-(N,P-GQDs)

To evaluate radio-agent stability in human serum, 300 µL (about 11.1 MBq) of ^{99m}Tc-(N, P-GQDs) was added to 500 µL of fresh centrifuged human plasma at 37 °C. The study was developed by performing ITLC from mixture at determined time intervals (up to 24 h) to calculate RCP% [26].

Table 1: Distribution of each radio-ingredient in two different kinds of ITLC system.

ITLC system	Solvent	R_f = 0	R_f = 1
SG-TLC(1)	Acetone	Colloid + ^{99m}Tc-(N-GQDs)	$^{99m}TcO_4^-$
SG-TLC(2)	(H_2O: EtOH: Ammonia)	Colloid	$^{99m}TcO_4^-$ + ^{99m}Tc-(N,P-GQDs)

2.8 Determination the octanol-water partition coefficient

For the determination of the octanol-water partition coefficient (log *P*), 100 µCi of ^{99m}Tc-(N,P GQDs) was added to vigorous vortex mixing of octanol-water mixture (2 mL, 1:1 v/v), and allowed to equilibrate at 37 °C. After 15 min, the %RCP of ^{99m}Tc-(N,P-GQDs) was calculated by ITLC through sampling from both phases (water and octanol) separately. The reported log *P* values were the average of the second and third extractions from three to four independent measurements. The log *P* was calculated by using the Equation (4), [27].

$$\log P = \log\left(\frac{\%^{99m}\text{Tc} - (\text{N, P} - \text{GQDs})\text{ in Octanol}}{\%^{99m}\text{Tc} - (\text{N, P} - \text{GQDs})\text{ in Water}}\right) \quad (4)$$

2.9 Evaluation of the ^{99m}Tc-(N,P-GQDs) particle size as nano radio-complex

Through Millipore membrane filter, 0.1 µm pore size, the particles size of radio-complex was estimated to assay if the radio-complex is considered as nano structure. The ^{99m}Tc-(N,P-GQDs) was passed throughout the filter by 5 mL syringe. The eluate (filtered mixture) and the syringe were counted in well counter to determine particle size based on their distribution. Furthermore, the eluate was investigated by ITLC to assay the RCP% in comparison with reaction mixture.

2.10 Evaluation of N,P-GQDs cell toxicity

We assessed the toxicity of N,P-GQDs against MCF-7 and MCF-10A as epithelial human breast cancer and non-malignant breast epithelial cell lines, respectively, using a primary MTT [3-(4,5-dimethylthiazol-2 yl)-2,5-diphenyltetrazolium bromide] cell viability method [28–31]. The cells were seeded into 96-well cell culture plate with a cell density of 4×10^3 and incubated in Dulbecco's Modified Eagle Medium (DMEM) and Roswell Park Memorial Institute (RPMI) medium or RPMI-1640 media for 24 h under 5 % CO_2 at 37 °C. The cells were then subjected to the test sample solutions of N,P-GQDs with different concentrations (0 (as control group), 0.01, 0.1, 1, 10, 50, 100 and 200 µg mL^{-1}). The treated cells were incubated for further 24 and 48 h. After removing the culture media solutions and washing the cells with PBS for three times, 200 µL of MTT solution (5 mg mL^{-1}) was added to each well and the medium was shaken for 4 h. Then, the MTT solution was replaced with 200 µL of DMSO per well. The viabilities of the treated cells in each well were measured using the optical density (OD) of the wells in an ELISA plate reader (Stat Fax 2100, USA) at 570 nm, and normalized to the untreated control cells by Equation (5):

$$\text{Survival fraction }(\%) = \left[\left(\text{OD}_{\text{sample}} - \text{OD}_{\text{blank}}\right) / \left(\text{OD}_{\text{control}} - \text{OD}_{\text{blank}}\right)\right] \times 100 \quad (5)$$

2.11 Relaxivity measurement of N,P-GQDs

To determine the potential application of the N,P-GQDs as MRI contrast agent, MRI measurements were performed using a 1.5 T MRI scanner (Prisma, Siemens Healthcare, Erlangen, Germany) with head and neck coil at room temperature. The N,P-GQDs NPs were dispersed in an agarose gel in the MRI phantom model at various phosphorus (P) concentrations measured by XPS results (0.04, 0.08, 0.16, 0.32, 0.16, 1.28, and 0.64 mM) according to XPS results. Dotarem® was prepared at the same concentrations as a control group. The T_1-weighted images were achieved using a conventional spin echo sequence with the following parameters: TR/TE = 50, 200, 400, 600, 800, 1100, 1300, 1500, 1800, 2000/11 ms, slice thickness = 5 mm, field of view (FOV) = 250 mm × 250 mm, 128 × 128 mm^2 field of view, and 256 × 256 matrix size. After image acquisition, the signal intensities of regions of interest (ROI) were defined by ImageJ software (version 1.41o). T_1 relaxation rates (R_1) was determined using best fitting of monoexponential functions. Finally, the r_1 relaxivity was determined through the linear curve fitting of R_1 ($1/T_1$) versus the P concentration [22, 32–35].

2.12 *In vitro* MRI N,P-GQDs

By treating MCF-7 and MCF 10A cells (5×10^6 cells/well) with various concentrations of N,P-GQDs (0, 1, and 10 µg mL^{-1}) for 6 h at 37 °C, it was determined if NPs target certain cell types. Before MRI, the cells were resuspended in PBS buffer at a cell density of 1×10^6 cells/mL. After incubation with determined concentration of N,P-GQDs, the cells were washed three times with PBS buffer and MRI measurements were performed by 1.5 T MRI machine (1.5 T Siemens, USA). Using a traditional spin-echo sequence, T_1-weighted MR images were obtained with the following settings: TR/TE = 500/12 ms, 220 × 320 matrices, 82 × 120 mm field of view, 140 Hz/Px of bandwidth, and a slice thickness of 3 mm. A monoexponential fitting approach was then used to estimate R_1 ($1/T_1$) values.

2.13 Animal treatment

Female healthy Wistar rats, at aged 4–5 months and weighing 200–230 g, were used in this investigation. The rats were treated under the standard conditions of feeding, temperature, and laboratory cages for 24 h prior to injection by radiotracer.

2.14 *In vivo* scintigraphy imaging study of Technetium-99m radiolabeled N,P-GQDs (^{99m}Tc-(N,P-GQDs))

Generally, three rats were injected with 3.7 MBq (100 µCi) up to 300 µL of ^{99m}Tc-(N,P-GQDs) in order to perform whole body scintigraphy. The selected rats were sedated by 60 mg/kg intraperitoneal (IP) injection of ketamine and fixed on an imaging board. The scintigraphy was performed at 30, 60, 120, 180, 240, 300, and 360 min after injection, by a dual-head SPECT system. (The gamma camera specifications are: Model: Siemens – E-CAM – Dual Head Gamma Camera, crystal size: 591 mm × 445 mm, thickness: 9.5 mm, PM Tubes: 95, Collimator: low energy high resolution). The board was adjusted to the heads of the camera, and the scan was performed. The mouse-to-head distance was 10 cm. The useful field of view (UFOV) was 533 mm × 387 mm. The matrix of pictures was 256 × 256 pixels. The spatial resolution was 10 mm FWHM at the CFOV.

3 Results

3.1 Characterization of N,P-GQDs

Some characterization employed techniques to identify the synthesized N,P-GQDs. The FT-IR spectroscopy showed a broad absorption band between 3400 and 3600 cm^{-1} related to the stretching vibrations of the –NH and –OH functional groups. The signals at 2854 and 2920 cm^{-1} are related to stretching vibrations of =C–H (or C–H) in the methylene group. The signals around 1738 and 1461 cm^{-1} are assigned to the stretching vibrations for the OC=O (carbonyl) and C–O (acidic) groups, respectively. The stretching vibration of C=C groups is at 1637 cm^{-1}. Also, signals at 1545 and 1385 cm^{-1} are related to N–H and C–N respectively. The signals at 1174 cm^{1} are related to stretching vibrations of P=O and the small bands at 1026 cm^{-1} indicate the stretching vibrations of the P–O groups in N,P-GQDs (Figure 2a). Because the GQDs are amorphous with special interlayer spacing, the XRD was used to identify the structure of the N,P-GQDs. The result showed the structure is amorphous and a broad peak appeared around 21.0°, which corresponded to an interlayer spacing of N,P-GQDs (3.93 Å) (Figure 2b). The thermal properties of N,P-GQDs were investigated using thermogravimetric analysis (TGA). The result shows that the weight loss occurs in the range 150–250 (Figure 2c), and the differences between this result and TGA of similar derivatives could be used to confirm the new synthesis. Concerning photoluminescence properties of the GQDs derivatives, the optical properties of N,P-GQDs were studied by photoluminescence spectroscopy. As shown in the result, the optimal emission peak at 480 nm appeared at an excitation wavelength of 382 nm, so it exhibits a green luminescence under PL (photoluminescence) irradiation (Figure 2d). X-ray photoelectron spectroscopy was performed to investigate the constituents of N,P-GQD. The XPS survey scan spectrum of the N,P-GQDs and high resolution XPS spectra of P 1s (phosphorus), C 1s (carbon), N 1s (nitrogen), and O 1s (oxygen) are illustrated in (Figure 2e_1–e_5). The survey spectrum shows the peaks at 192.38, 285.08, 400.08 and 532.08 eV, corresponding to P1, C1, N1, and O1 respectively (Figure 2e_1). The high-resolution XPS spectrum of O 1s illustrates two peaks at 531.98 and 533.38 eV related to C=O and C–O, respectively (Figure 2e_2). The N 1s peaks at 400.28 and 401.88 eV correspond to the C–N and N–H functional groups (Figure 2e_3). The C 1s peaks at 285.08, 286.88 and 288.68 eV can be assigned to C=C, C–N/C–O, and C=O, respectively (Figure 2e_4). In the high-resolution spectrum of P 1s, the peak at 192.38 eV is assigned to P–O. The atomic percentages were calculated as P 1s: 1.2 %, C 1s: 57.34 %, N 1s: 8.73 %, and O 1s: 32.73 % (Figure 2e_5). The morphology of the synthesized N,P-GQDs was assayed using transmission electron microscopy (TEM). The results showed a spherical structure sized about 10 nm (Figure 2d).

3.2 Factors affecting the radiolabeling yield of N,P-GQDs

Some involved factors' changes including temperature, pH, amount of ligand and reducing agents can affect the radiolabeling process and improve %RCP effectively. Therefore, the effect of each involved factor was investigated during the Technetium-99m radiolabeling reaction.

3.3 The effect of pH

For the investigation of pH effects on radiolabeling reaction, the process was performed at pH 1–8. The involved factors were fixed (as 10 mg of N, P-GQDs, 100 µL of $SnCl_2$, 74 MBq of $^{99m}TcO_4^-$, temperature: 95 °C). The %RCP calculation in the acidic range (1–3) showed that the radiolabeling yield was ≤15 % and the $^{99m}TcO_4^-$ was reduced to colloid completely. The maximum amount of %RCP was studied at pH ≥ 4 up to pH 6–6.5. Also, a high pH (up to 12), decreased %RCP following a high percentage of the hydrolyzed-reduced technetium-99m. Considering the other fixed factors, the %RCP was increased to almost 70 % in the pH range of 6–7 (Figure 3a).

3.4 The effect of $SnCl_2{\cdot}2H_2O$ (reducing agent) concentration

For ^{99m}Tc-radiolabeling of N,P-GQDs nano-structures, the $^{99m}TcO_4^-Na^+$ (Tc-99m (+7) pertechnetate) milked from the $^{99}Mo/^{99m}Tc$ generator should be reduced to a possibly lower oxidation state (depending on the chelate and conditions) for radiolabeling with chelate (ligand). Generally, $SnCl_2$ has been used for this purpose as potent reductant. Under the constant conditions of other factors (10 mg of N,P-GQDs, 37 MBq of $^{99m}TcO_4^-$, pH = 6.5 and temperature: 95 °C), we used different concentrations of stock solution of $SnCl_2$ (50–200 µL) and followed the %RCP with ITLC. The results showed that about 100 µL of the stock solution could reduce 37 MBq of $^{99m}TcO_4^-$ completely. The high concentration (≥150 µL) could increase the amount of colloid (Figure 3b).

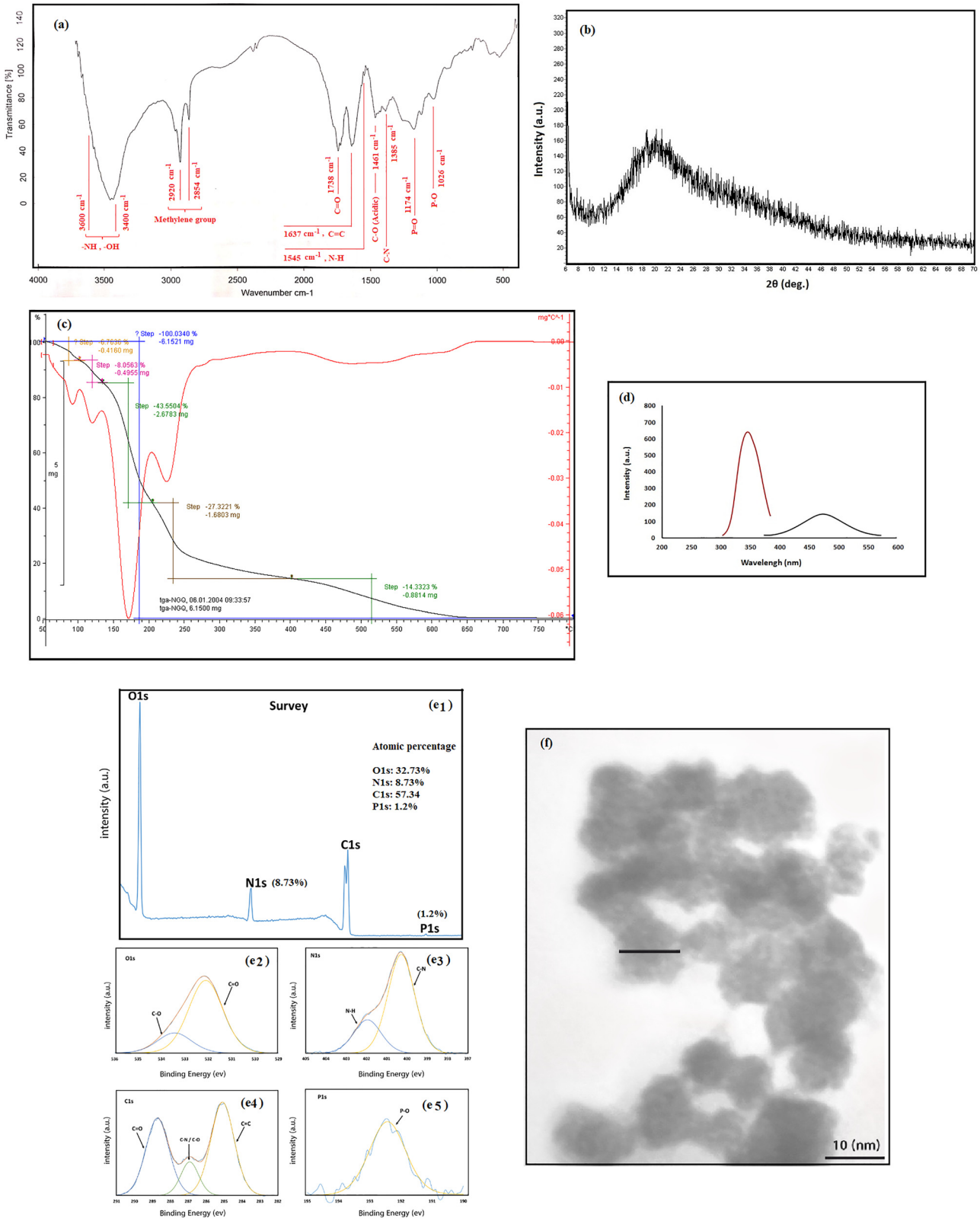

Figure 2: (a) FT-IR spectrum of N,P-GCDs at room temperature, (b) XRD patterns of N,P-GCDs. As the Figure shows interlayer spacing is concluded at 3.93 Å, (c) TGA analyses of N,P-GQDs, (d) fluorescence microscopy spectra of N,P-GCDs, (e_1–e_5) the XPS survey scan spectrum of the N,P-GQDs and high resolution XPS spectra of O 1s, N 1s, C 1s, and P 1s, (f) TEM image of the synthesized N,P-GCDs. As it shows the size of nanoparticles is 10≥ nm.

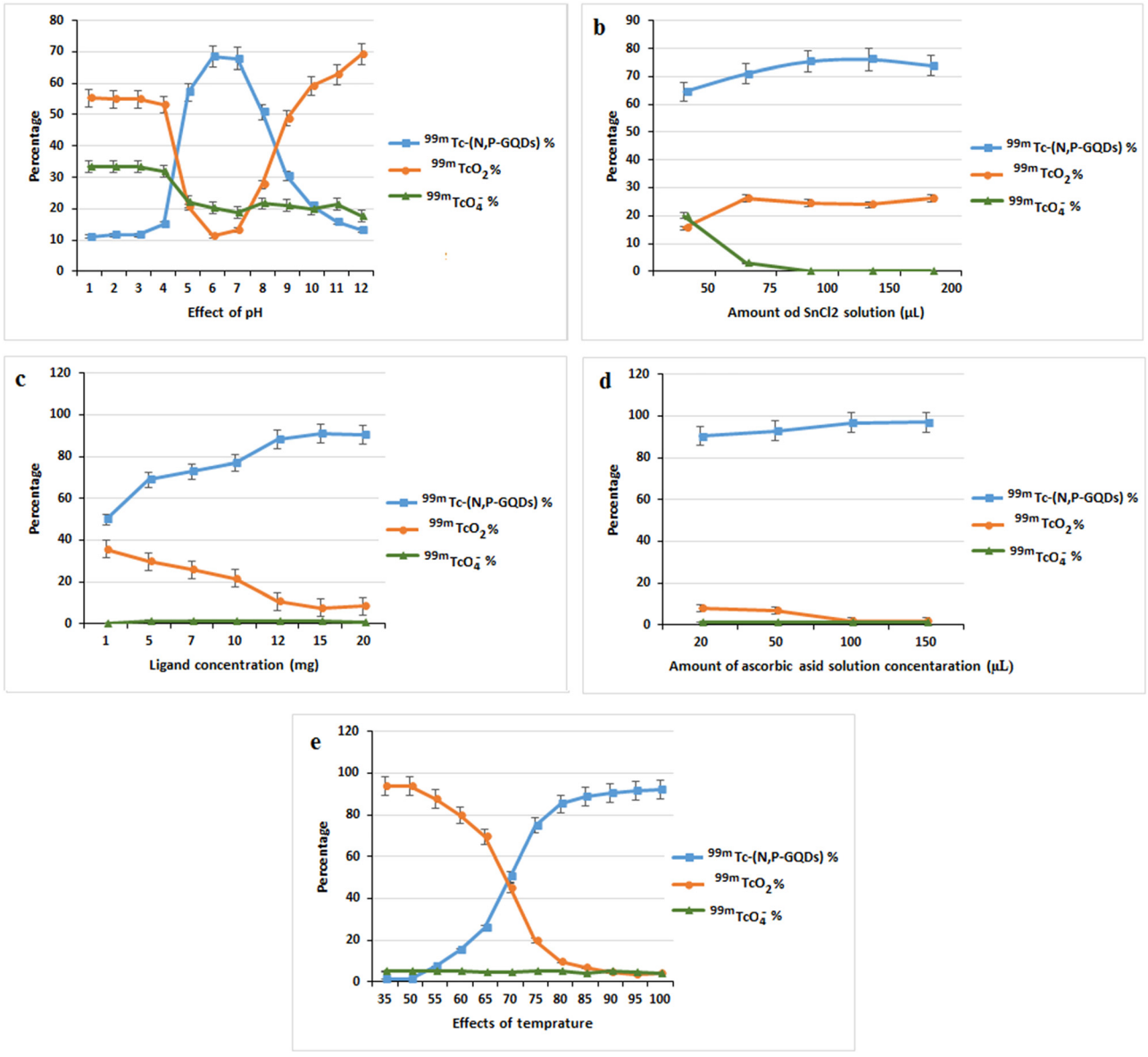

Figure 3: (a) The effect of pH on the radiolabeling of N,P-GQDs with Technetium-99m. pH = 6.5 was preferable in this process, (b) the effect of $SnCl_2{\cdot}2H_2O$ concentrations on radiolabeling of N,P-GQDs, (c) the effect of N,P-GQDs concentration on the radiolabeling process, (d) the effect of ascorbic acid concentration on the radiolabeling of N,P-GQDs, (e) the effect of temperature on radiolabeling process. As it is illustrated, under the optimum conditions of all other variables, increasing the temperature to 95 °C, could raise the %RCP.

3.5 The effect of N,P-GQDs concentrations

To achieve an optimal concentration of N,P-GQDs as a ligand, several concentrations ranging from 1 mg to 20 mg were utilized in the process of radiolabeling. %RCP was performed after ITLC. The optimum amount was achieved with 15 mg of N,P-GQDs, 37 MBq of $^{99m}TcO_4^-$, pH = 6.5, $SnCl_2$ 100 µL, and a temperature of 95 °C (Figure 3c).

3.6 The effect of acid ascorbic concentrations

Some ^{99m}Tc-radiolabeling processes may be improved by using acid ascorbic as an antioxidant agent that could control the auto-radiolysis process during the radiolabeling reaction and raise the %RCP. During this study, the radiolabeling was done at different concentrations of acid

ascorbic stock solution (20–200 µL). The RCP≥ %95 was obtained with 100 µL of acid ascorbic stock solution (Figure 3d).

3.7 The effect of temperature

In order to assay the effect of temperature on the radiolabeling reaction, the process was performed in a temperature range of 40–100 °C. The study showed that performing the reaction at high temperatures (95–100 °C) works for this radiolabeling process. Under the instant conditions of the involved factors (15 mg of N, P-GQDs, 100 µL of $SnCl_2$, 37 MBq of $^{99m}TcO_4^-$, 100 µL of acid ascorbic stock solution, and pH = 6.5), the %RCP reaches about 96 % (Figure 3e). It should be mentioned that $^{99m}TcO_4^-$ is reduced by $SnCl_2$ at each temperature, depending on the reducing agent ($SnCl_2$) concentration.

3.8 Serum stability assay of ^{99m}Tc-(N,P-GQDs)

The fresh plasma from centrifuged healthy human blood was used to determinate ^{99m}Tc-(N,P-GQDs) serum stability. The 11.1 MBq of radiolabeling reaction was added to a vial with plasma and left for 24 h at a room temperature. The ITLC was performed at a determined time up to 24 h. The results showed that the radio-complex was completely stable without significant Technetium-99m separation from the radiolabeled structure (Figure 4a).

3.9 Evaluation of radio-complex particle size as nano radio-complex

To determine the particles size of ^{99m}Tc-(N,P-GQDs), a 0.1 µm membrane filter was used. The mixture of reaction with % RCP ≥ 95 was injected into the 0.1 µm membrane filter by syringe. Both the eluate (filtered mixture) and filter were counted separately. The results showed 70.8 % of the mixture passed through the filter, so 70.8 % of particles in the mixtures were ≤0.1 µm (Figure 4b). Although, the particle size of N,P-GQDs was determined using TEM, there is a possibility of radio-complex aggregation. Hence, the subsequent step involves conducting ITLC using the eluate (the filtered mixture, indicated by orange) and an unfiltered

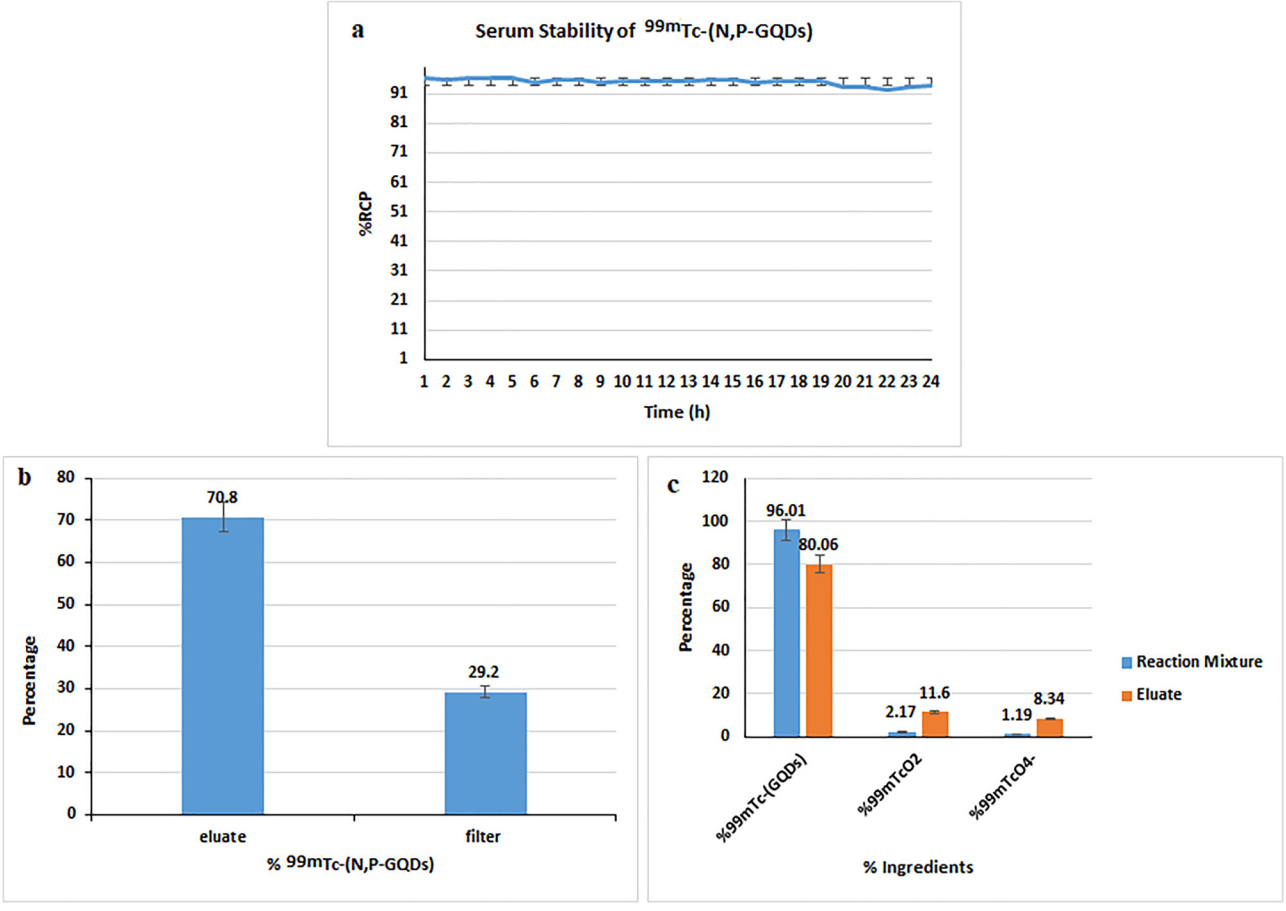

Figure 4: (a) Serum stability of ^{99m}Tc-(N,P-GQDs), (b) the percentage of radio-complex in eluate and filter, (c) percentage of each ingredient in reaction mixture and eluate comparatively.

mixture of reactions (indicated by blue). The results showed that $\%^{99m}TcO_4^-$ and $\%^{99m}TcO_2$ were raised in eluate because of their small sizes in comparison to the radio-complex (Figure 4c).

3.10 Determination of the octanol/water partition coefficient (log *P*)

The hydrophobicity/hydrophilicity property of ^{99m}Tc-(N,P-GQDs) was determined by calculating the log *P* value, which was found to be –2.9. The results showed that the radio-complex diffused in the water phase because of the presence of polar functional groups indicating that ^{99m}Tc-(N,P-GQDs) has a hydrophilic structure and is likely to be removed by the renal system.

3.11 Cell viability of N,P-GQDs

The results of the cytotoxicity assay showed that there is no obvious decrease in cell viability with various concentrations of N,P-GQDs (0(control group)-200 µg/mL) for 24 h incubation time (Figure 5a). Even at the concentration of 200 µg/mL, the cell viability still remained above 90 %. Increasing the incubation time of the NPs to 48 h, the cell survival rate decreases with a concentration-dependent trend and shows a non-significant reduction in cell viability in comparison to the control group (Figure 5b). Nevertheless, N,P-GQDs NPs exhibited reduced cytotoxicity towards MCF 10A (the non-malignant cell line) compared to MCF-7 (the cancerous cell line) when both were exposed to a concentration of 200 µg/mL. However, this result was not statistically significant, possibly due to the high accumulation of the prepared N,P-GQDs NPs in cancerous cells compared with normal cells. This resulted in their specific cell uptake through the enhanced permeability and retention (EPR) mechanism. These results indicated that N,P-GQDs could have little cytotoxicity at the given concentration range, which is essential for further *in vitro* and *in vivo* imaging and biological applications.

3.12 Relaxivity of N,P-GQDs as MRI contrast agents

The N,P-GQDs NPs showed slightly brighter T_1 weighted images than a commercially approved MRI contrast agent (Dotarem®) in the phantom model. The N,P-GQDs were found to efficiently shorten the longitudinal relaxation time (T_1) and significantly increase signal intensity in T_1-weighted

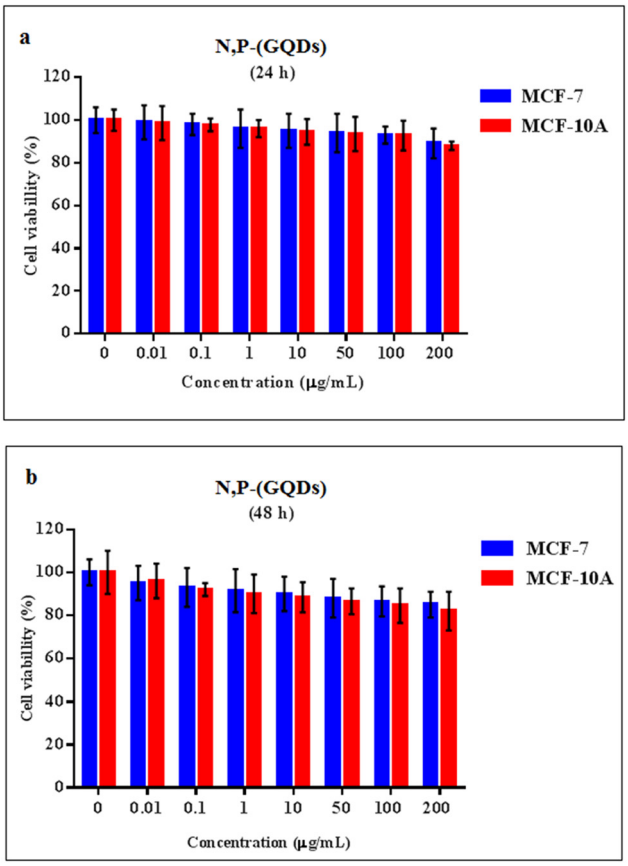

Figure 5: (a) MCF-7 and MCF-10A cells viability after treatment with N,P-GQDs NPs in different concentrations after 24 h of incubation, (b) MCF-7 and MCF-10A cells viability after treatment with N,P-GQDs NPs in different concentrations after 48 h of incubation.

images in comparison with, Dotarem® (Figure 6a). However, the degree of the bright contrast enhancement in T_1-weighted images for all groups was found to be directly related to the concentration of phosphate ions. The r_1 relaxivity values for N,P-GQDs and Dotarem® were respectively achieved at 4.49 $mM^{-1}\,s^{-1}$ and 2.54 $mM^{-1}\,s^{-1}$ as shown in (Figure 6b). In comparison to Dotarem®, it was revealed that the N,P-GQDs NPs effectively reduced the longitudinal relaxation time (T_1) and greatly increased signal intensity in T_1-weighted images. However, it was observed that the amount of bright contrast increasing in T_1-weighted images for all groups was correlated with the phosphor ion concentration.

Contrast agents made from graphene, specifically graphene dots doped with heteroatoms, utilize carbon bonds with heteroatoms to function as magnetic centers. These magnetic dipoles can interact with water molecules, leading to a modification in the spin relaxation time of hydrogen atoms in the region where the contrast material is located. Consequently, this amplifies the resulting signal and enables

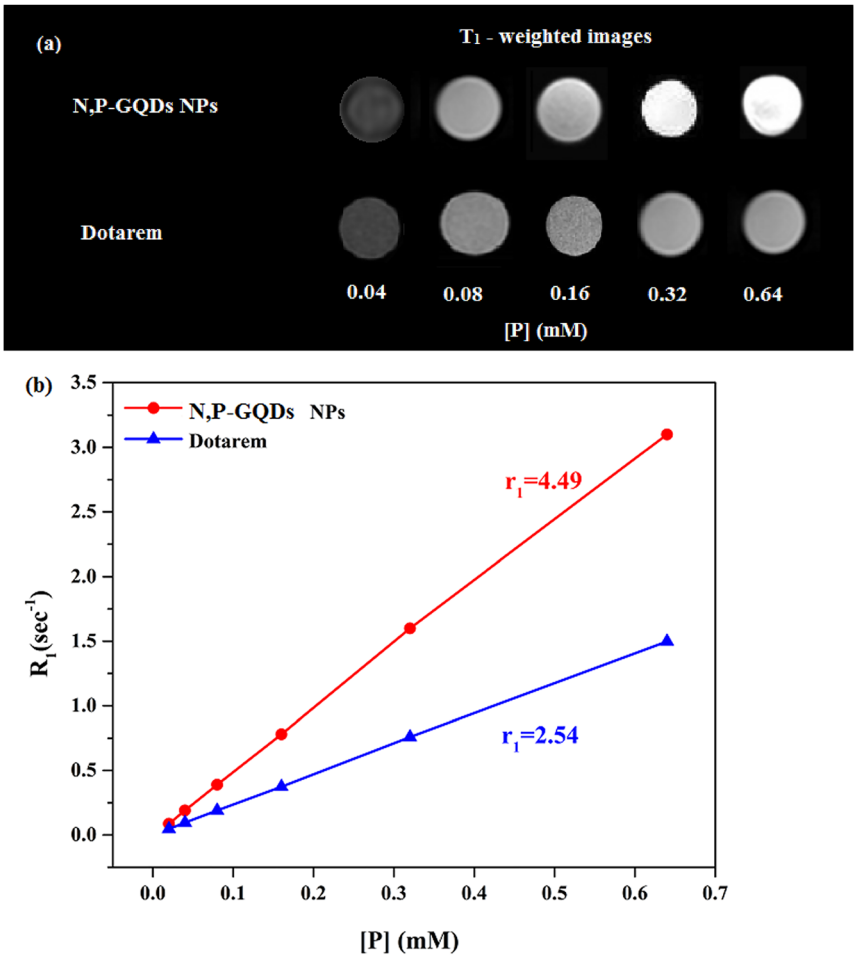

Figure 6: (a) T1 – weighted images of N,P-GQDs NPs and Dotarem® as a clinically available contrast agent with various concentrations in water phantom. (b) The longitudinal relaxivity (r1) relaxivity of N,P-GQDs NPs and Dotarem® at different concentration values.

the production of magnetic resonance images. This mechanism exhibits similarities to the paramagnetic property observed in paramagnetic metal ions. However, it is noteworthy that this feature is observed even in the absence of metal ions, which is particularly relevant in terms of toxicity. The nano-scale structure enhances the quantity of functional atoms involved in MRI signal generation, hence increasing the number of paramagnetic centers [2, 3, 36].

3.13 *In vitro* MRI measurements

In order to confirm the cancer cell targeting ability of the N,P-GQDs NPs and MR imaging performance, both MCF-7 and MCF 10A cells were incubated with the particles in different concentrations (0, 10 and 50 µg/mL) for 6 h. As shown in (Figure 7), the T_1-weighted MR images showed a significant enhancement in MCF-7 cells. The R_1 value of MCF-7 cells was about three times greater than that of the untreated control cells when treated with N,P-GQDs NPs (50 µg/mL) for 6 h, as a result of the quantitative analysis of the MR signal change. However, under the same condition, the R_1 of MCF-10A cells was only 1.4 times greater than the untreated control cells. The particular cellular uptake of the N,P-GQDs NPs into MCF-7 cells as a result of greater cell division and activity in comparison to MCF-10A normal cells may be attributed to the considerable difference between MCF-7 and MCF-10A cells in MRI.

3.14 *In vitro* MRI evaluations

As shown in (Figure 7a), the T_1-weighted MR images showed a significant enhancement in MCF-7 cells. The R_1 value of MCF-7 cells was around three times greater than that of the untreated control cells when treated with N,P-GQDs NPs (50 µg/mL) for 6 h, according to a quantitative analysis of the MR signal change. However, under the same condition, the R_1 of MCF-10A cells was only 1.4 times greater than that of untreated control cells (Figure 7b).

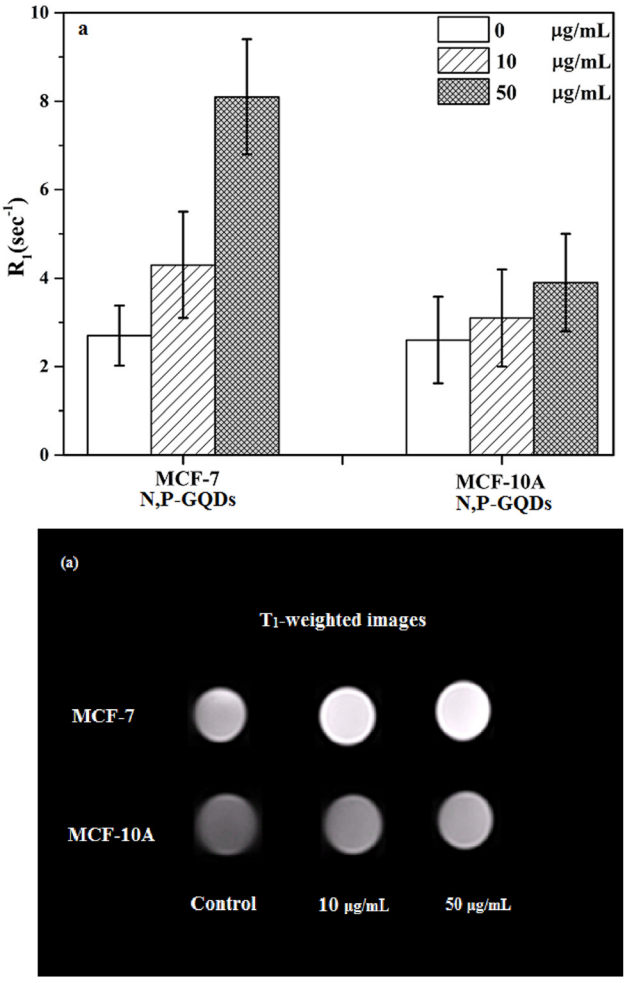

Figure 7: (a) Longitudinal relaxation rate at cells treated with different N,P-GQDs NPs concentration. (b) T1 – weighted MRI images of N,P-GQDs NPs in MCF-7 and MCF 10A cells at different concentration of NPs after 6 h incubation time on 1.5 T MR system.

3.15 *In vivo* scintigraphy imaging studies

The rats were treated and administered by the ^{99m}Tc-(N,P-GQDs) radiotracer through the caudal vein and scintigraphy imaging was performed for up to 6 h. As soon as the rats were injected, the radiotracer diffused throughout the circulatory system and kidneys. Up to 30 min after injection, the blood and renal systems were obvious (Figure 8a). As time passes, the soft tissues are cleared from the radiotracer by the kidneys elimination. Therefore, the renal system, especially the bladder and kidneys, are considered risk organs up to 4 h after injection (Figure 8b–d). Five hours after injection, the bladder is evacuated by urination, and after 6 h the bladder is firmly empty in spite of the kidneys retention of the radiotracer (Figure 8e and f). Because of the ^{99m}Tc-(N,P-GQDs) concentration in the kidneys until 6 h after injection, it is guessed the radio-agent is bound to the kidney cortex in addition to elimination through filtration/secretion mechanisms in the kidneys.

4 Discussion

During this study the N,P-GQDs were synthesized by synthetic microwave, characterized through common characterization methods, and studied to see if they had the potential to be considered as dual imaging agents for MRI and scintigraphy. The N,P-GQDs were radiolabeled with fresh $^{99m}TcO_4^-$ from the ^{99}Mo/^{99m}Tc generator as ^{99m}Tc-(N,P-GQDs). All affecting variables in the radiolabeling process were studied to improve RCP to reach ≥95 %. It seems new radiocomplexes are going to be of interest in different fields, especially imaging studies. After preparing of ^{99m}Tc-(N,P-GQDs) in good purity, the IV injection was performed on healthy female rats through the caudal vein. The ^{99m}Tc-(N,P-GQDs) circulated in the blood system, but the renal system eliminated them, as the imaging studies showed (Figure 8). Because the kidneys attract a substantial percentage of radio-complex, they remain a key organ during all evaluations following injection. Because of bladder evacuation 5 h after injection (Figure 8e and f), it was concluded that the renal cortex captured ^{99m}Tc-(N,P-GQDs) in addition to radio-complex clearance. In comparison to our previous work about ^{99m}Tc-(N-GQDs), which were cleared through both the kidneys and the colon, this study demonstrated that the ^{99m}Tc-(N,P-GQDs) are just cleared by the kidneys (14). The slight difference in log *P* values between the two radio-complexes, indicates that the phosphate group is responsible for biodistribution changes in new the radiocomplex. The imaging study demonstrated that ^{99m}Tc-(N,P-GQDs) is captured by kidneys but the mechanism has not been investigated. Because of their greater biocompatibility, low toxicity, high capacity, and smaller size, GQDs are noticed in different fields as well as in radiolabeling. Prior to the radiolabeling of GQDs, 131-I radiolabeled graphene oxide was prepared in order to perform mixed radiotherapy/photothermal therapy for breast cancer in mice [37]. B. Challan radiolabeled graphene oxide with 99m-Technetium for imaging of infection in rats because of the accumulation of graphene oxide in sites infected with microorganisms. Apparently, this radiotracer could differentiate between infection and sterile inflammatory sites [38]. Firstly, the GQDs were radiolabeled with 99m-Technetium through

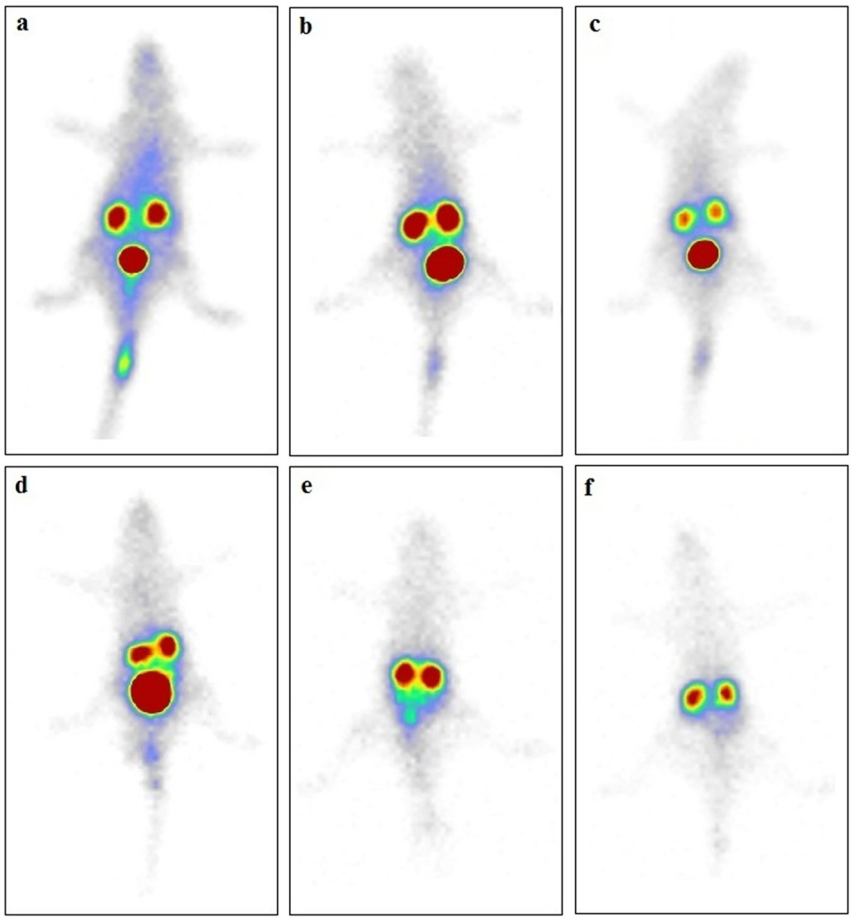

Figure 8: Scintigraphy imaging of iv injected normal female rats by ^{99m}Tc-(N,P-GQDs). (a) Up to 30 min blood system, soft tissue and renal system are obvious. (b–d) The radiotracer is cleared by renal system and the bladder received a higher amount of that in spite of soft tissues up to 4 h after injection. (e, f) The bladder is evacuated by urination but some percentage of the radiotracer is still captured by kidneys' cortex.

nitrogen doped GQDs as ^{99m}Tc-(N-GQDs). During the study, it was shown that the N-GQDs could be efficiently radiolabeled with 99m-Technetium. The biodistribution studies demonstrated that ^{99m}Tc-(N-GQDs) are mostly eliminated by the kidneys, and a low amount of that is cleared by the liver and accumulated in the colon [14]. Yang Yang et al. radiolabeled GQDs with 223-Radium (a common alpha-emitting radioisotope used in clinics) as an internal radiotherapy target against osteosarcoma cells (MG63 and SAOS2). This study found that the ^{223}Ra-GQDs are attracted to the lesions and affect them prominently. Furthermore, Radium-223 chloride (Alpharadin/Xofigo) is used for therapy of bone metastasis due to breast and castrate-resistant prostate cancer because of the $^{223}Ra^{+2}$ concentration in bone metastasis. So, it is guessed that the GQDs just improve the radioisotope concentration in bone lesions. Following that, during both our investigations on the preparation of ^{99m}Tc-(N-GQDs) and 99mTc-(N,P-GQDs), it was concluded that these radiolabeled GQDs derivatives are not concentrated in bone. Also, they are eliminated by kidneys and colon depending on their functional groups. So, it was estimated that the retention of ^{223}Ra-GQDs in the skeletal system is related to 223-Radium instead of GQDs structure [39]. Relaxivity measurements exhibited that our produced NPs have a stronger T_1 shortening effect and can be used as positive MRI contrast agents because of their higher r_1 value and prominently displayed concentration-dependent signal intensity effect. In this study, Dotarem® was used as a control group as a commercially available CA for T_1 relaxation time in numerous studies. Various r_1 have been reported for Dotarem® from 0.75 to 4.89 $mM^{-1}s^{-1}$ according to the experimental conditions [40]. The reduction in positive contrast enhancement of Dotarem® in comparison with prepared NPs could be due to the extracellular performance of this standard contrast agent. In the study by Rohrer et al., the magnetic properties of MRI contrast media solutions at different magnetic field strengths were compared, and the relaxivity for Dotarem® on 1.5 T has been described as $r_1 = 2.9\ mM^{-1}s^{-1}$ and $r_2 = 3.2\ mM^{-1}s^{-1}$ [41]. The r_1 value depends on various factors including the type of NPs, hydrodynamic diameter, and the properties of the ligands or coating agents surrounding the doped element. Furthermore, additional research is required to determine the optimal thickness of the coating layer and particle size of the MRI contrast agent. Furthermore,

although it is reported that introducing Gd into carbon dots could increase the relaxivity of carbon dots, the r_1 relaxivity of the synthesized N,P-GQDs NPs is still greater than reported Gd-carbon dots [42]. These results suggest that phosphorus doping is more efficient than metal doping in carbon-based materials in enhancing relaxivity. This may be due to the smaller diameter of doped ions atoms that produce more paramagnetic centers in nanostructured carbon materials. The N,P-GQDs, NPs as a novel metal-free contrast agent provide contrast enhancement in T_1-weighted imaging and may have a significant implication in medical imaging. As claimed by the *in vitro* MRI analysis in both normal and cancerous cell lines, the particular cellular uptake of the N,P-GQDs NPs into MCF-7 cells as a result of greater cell division and activity in comparison to MCF-10A normal cells may be attributed to differential diagnosis between MCF-7 and MCF-10A cells in MR imaging. Taken together, it was worth a try to apply the prepared N,P-GQDs NPs for detecting cancerous cells (as differential diagnosis) because of the acidic microenvironment of the tumor tissue. It is suggested that future studies assess the accumulation of ^{99m}Tc-(N-GQDs) to the significant difference between the concentrations of N,P-GQDs in MCF-7 and MCF-10A cells in MRI investigations.

5 Conclusions

During this study, it was concluded that the synthesized N,P-GQDs NPs have the ability to be radiolabeled with Technetium-99m radio-isotope as *in vitro* and *in vivo* stable ^{99m}Tc-(N,P-GQDs). The *in vivo* investigations showed the radio-complex is eliminated and captured by the kidneys. The distinct biodistribution of 99mTc-(N,P-GQDs) compared to 99mTc-(N-GQDs) indicates that the presence of different doped atoms in GQDs has the potential to alter the biodistribution. Lack of significant cytotoxicity, following MTT assay against normal (MCF-10A) and cancerous (MCF-7) human breast cell line, the N,P-GQDs NPs could be confidently used for *in vivo* studies. Also, the relaxivity measurement of N,P-GQDs as MRI contrast agents showed the N,P-GQDs NPs can be considered metal-free MRI contrast agents because they have high relaxivity in comparision to clinically applied contrast agents. The different uptake of N,P-GQDs NPs into MCF-7 and MCF-10A cells that was resulted from *in vitro* MRI evaluations, suggested that the N,P-GQDs could be used in differential diagnosis between the two mentioned cells, but *in vivo* MRI research is definitely necessary. Based on this study, it was generally concluded that the N,P-GQDs have the potential to be introduced as new nanoagents to the realms of imaging, especially MRI and scintigraphy, for different purposes.

Acknowledgments: We thank the Tabriz University of Medical Sciences, Medical Radiation Sciences Research Team and Islamic Azad University, Science and Research Branch for officially supporting us. We also thank Dr. Ashkan Shomali and Azadeh Ostadchinigar, and Shimi Sanat Nano Tech. Co. for expert consultation on the synthesis of N,P-GQDs and interpretation of the analysis, Dr. Shahram Dabiri for his contribution to performing scintigraphy and Habib Rahnema for his assistance with reviewing and editing this article. We would like to appreciate of the cooperation of Clinical Research Development Unit, Imam Reza General Hospital, Tabriz, Iran in conducting of this research.

Research ethics: The study was approved by the Medical Radiation Sciences Research Team and Research Ethics Committee (REC) of Tabriz University of Medical Sciences, Iran. (Code:IR.TBZMED.AEC.1402.049).

Author contributions: MM, AF and TM designed the reseach and collected the data. MM, AF, TM and FBM processed and interpreted the data and drafted the manuscript. AJN reviewed the manuscript. All authors read and approved the final manuscript.

Competing interests: The authors declare that they have no competing interests.

Research funding: None declared.

Data availability: Not applicable.

References

1. Chenthamara D., Subramaniam S., Ramakrishnan S. G., Krishnaswamy S., Mohamed Essa M., Lin F. H., Qoronfleh M. W. Therapeutic efficacy of nanoparticles and routes of administration. *Biomater. Res.* 2019, *23*(20), https://doi.org/10.1186/s40824-019-0166-x.
2. Yan Y., Gong J., Chen J., Zeng Z., Huang W., Pu K., Liu J., Chen P. Recent advances on graphene quantum dots: from chemistry and physics to applications. *Adv. Mater.* 2019, *31*(21), https://doi.org/10.1002/adma.201808283.
3. Chung S., Revia R. A., Zhang M. Graphene quantum dots and their applications in bioimaging, biosensing, and therapy. *Adv. Mater.* 2021, *33*(22), https://doi.org/10.1002/adma.201904362.
4. Mansuriya B. D., Altintas Z. Applications of graphene quantum dots in biomedical sensors. *Sensors* 2020, *20*(4), https://doi.org/10.3390/s20041072.
5. Zhang P., Huang Y., Lu X., Zhang S., Li J., Wei G., Su Z. One-step synthesis of large-scale graphene film doped with gold nanoparticles at liquid–air interface for electrochemistry and Raman detection applications. *Langmuir* 2014, *30*(29), https://doi.org/10.1021/la5024086.

6. Jiang D., Chen Y., Li N., Li W., Wang Z., Zhu J., Zhang H., Liu B., Xu S. Synthesis of luminescent graphene quantum dots with high quantum yield and their toxicity study. *PLoS One* 2015, *10*(12), https://doi.org/10.1371/journal.pone.0144906.
7. Biswas M. C., Islam M. T., Kumar Nandy P., Milon Hossain M. Graphene quantum dots (GQDs) for bioimaging and drug delivery applications: a review. *ACS Mater. Lett.* 2021, *3*, 889–911.
8. Xue Z., Sun Q., Zhang L., Kang Z., Liang L., Wang Q., Shen J. W. Graphene quantum dot assisted translocation of drugs into a cell membrane. *Nanoscale* 2019, *11*, 4503–4514.
9. Iannazzo D., Pistone A., Salamò M., Galvagno S., Romeo R., Giofré S. V., Branca C., Visalli G., Di Pietro A. Graphene quantum dots for cancer targeted drug delivery. *Int. J. Pharm*. 2017, *25*, 185–192.
10. Wang C., Wu C., Zhou X., Han T., Xin X, Wu J., Zhang J., Guo S. Enhancing cell nucleus accumulation and DNA cleavage activity of anti-cancer drug via graphene quantum dots. *Sci. Rep.* 2013, *3*, 2852.
11. Yang H. W., Huang C. Y., Lin C. W., Liu H. L., Huang C. W., Liao S. S., Chen P. Y., Lu Y. J., Wei K. C., M Ma C. C. Gadolinium-functionalized nanographene oxide for combined drug and microRNA delivery and magnetic resonance imaging. *Biomaterials* 2014, *35*, 6534–6542.
12. Cheong W. F., Prahl S. A., Welch A. J. A review of the optical properties of biological tissues. *IEEE J. Quantum Electron.* 1990, *26*, 2166–2185.
13. Ballou B., Ernst L. A., Waggoner A. S. Fluorescence imaging of tumors *in vivo*. *Curr. Med. Chem*. 2005, *12*, 795–805.
14. Gharepapagh E., Fakhari A., Firuzyar T., Shomali A., Azimi F. Preparation, biodistribution and dosimetry study of Tc-99m labeled N-doped graphene quantum dot nanoparticles as a multimodular radiolabeling agent. *New J. Chem.* 2021, *45*, 3909–3919.
15. Ruth T. J. The shortage of technetium-99m and possible solutions, the annual review of nuclear and particle science. *Annu. Rev. Nucl. Part. Sci*. 2020, *70*, 77–94.
16. Mortezazadeh T., Gholibegloo E., Alam N. R., Dehghani S., Haghgoo S., Ghanaati H., Khoobi M. Gadolinium (III) oxide nanoparticles coated with folic acid-functionalized poly (β-cyclodextrin-co-pentetic acid) as a biocompatible targeted nano-contrast agent for cancer diagnostic: *in vitro* and *in vivo* studies. *MAGMA* 2019, *32*, 487–500.
17. Chen H., Wang G. D., Tang W., Todd T., Zhen Z., Tsang C., Hekmatyar K., Cowger T., Hubbard R. B., Zhang W., Stickney J., Shen B., Xie J. Gd-encapsulated carbonaceous dots with efficient renal clearance for magnetic resonance imaging. *Adv. Mater.* 2014, *26*, 6761–6766.
18. Rogosnitzky M., Branch S. Gadolinium-based contrast agent toxicity: a review of known and proposed mechanisms. *BioMetals* 2016, *29*, 365–376.
19. Gupta A., Caravan P., Price W. S., Platas-Iglesias C., Gale E. M. Applications for transition-metal chemistry in contrast-enhanced magnetic resonance imaging. *Inorg. Chem.* 2020, *59*, 6648–6678.
20. Fu C., Yu Y., Xu X., Wang Q., Chang Y., Zhang C., Zhao J., Peng H., Whittaker A. K. Functional polymers as metal-free magnetic resonance imaging contrast agents. *Prog. Polym. Sci.* 2020, *108*, 101286.
21. Hu Y. H. The first magnetic-nanoparticle-free carbon-based contrast agent of magnetic-resonance imaging-fluorinated graphene oxide. *Small* 2014, *10*, 1451–1452.
22. Wang H., Revia R., Wang K., Kant R. J., Mu Q., Gai Z., Hong K., Zhang M. Paramagnetic properties of metal-free boron-doped graphene quantum dots and their application for safe magnetic resonance imaging. *Adv. Mater.* 2017, *29*, 1605416.
23. Wang H., Revia R., Mu Q., Lin G., Yena C., Zhang M. Single-layer boron-doped graphene quantum dots for contrast-enhanced *in vivo* T_1-weighted MRI. *Nanoscales Horiz.* 2020, *5*, 573–579.
24. Nair R. R., Sepioni M., Tsai I. L., Lehtinen O., Keinonen J., Krasheninnikov A. V., Thomson T., Geim A. K., Grigorieva I. V. Spin-half paramagnetism in graphene induced by point defects. *Nat. Phys.* 2012, *8*, 199–202.
25. Hu Y. H. The first magnetic-nanoparticle-free carbon-based contrast agent of magnetic-resonance imaging-fluorinated graphene oxide. *Small* 2014, *10*, 1451–1452.
26. Fakhari A., Jalilian A. R., Yousefnia H., Johari-Daha F., Mazidi M., Khalaj A. Development of ^{166}Ho-pamidronate for bone pain palliation therapy. *J. Radioanal. Nucl. Chem*. 2015, *303*, 743–750.
27. Kwon Y. *Handbook of Essential Pharmacokinetics, Pharmacodynamics and Drug Metabolism for Industrial Scientists;* Kluwer Academic/Plenum Publishers: New York, 2004. eBook.
28. Cai H., An X., Cui J., Li J., Wen S., Li K., Shen M., Zheng L., Zhang G., Shi X. Facile hydrothermal synthesis and surface functionalization of polyethyleneimine-coated iron oxide nanoparticles for biomedical applications. *ACS Appl. Mater. Interfaces* 2013, *5*, 1722–1731.
29. Marks D. C., Belov L., Davey M. W., Davey R. A., Kidman A. D. The MTT cell viability assay for cytotoxicity testing in multidrug-resistant human leukemic cells. *Leukemia Res.* 1992, *16*, 1165–1173.
30. Dehghani S., Hosseini M., Haghgoo S., Changizi V., Akbari Javar H., Khoobi M., Riahi Alam N. Multifunctional MIL-Cur@FC as a theranostic agent for magnetic resonance imaging and targeting drug delivery: *in vitro* and *in vivo* study. *J. Drug Target.* 2020, *28*, 1–13. Epub 2020 Jan 10.
31. Gholibegloo E., Mortezazadeh T., Salehian F., Forootanfar H., Firoozpour L., Foroumadi A., Ramazani A., Khoobi M. Folic acid decorated magnetic nanosponge: an efficient nanosystem for targeted curcumin delivery and magnetic resonance imaging. *J. Colloid Interface Sci.* 2019, *556*, 128–139.
32. Babić-Stojić B., Jokanović V., Milivojević D., Požek M., Jagličić Z., Makovec D., Arsikin K., Paunović V. Gd_2O_3 nanoparticles stabilized by hydrothermally modified dextrose for positive contrast magnetic resonance imaging. *J. Magn. Magn. Mater.* 2016, *403*, 118–126.
33. Pierre V. C., Allen M. J., Caravan P. Contrast agents for MRI: 30+ years and where are we going? *J. Biol. Inorg. Chem.* 2014, *19*, 127–131.
34. Mortezazadeh T., Gholibegloo E., Riyahi Alam N., Dehghani S., Haghgoo S., Ghanaati H., Khoobi M. Gadolinium (III) oxide nanoparticles coated with folic acid-functionalized poly(β-cyclodextrin-co-pentetic acid) as a biocompatible targeted nano-contrast agent for cancer diagnostic: *in vitro* and *in vivo* studies. *Magn. Reson. Mater. Phys.* 2019, *32*, 487–500.
35. Mansouri H., Gholibegloo E., Mortezazadeh T., Yazdi M. H., Ashouri F., Malekzadeh R., Najafi A., Foroumadi A., Khoobi M. A biocompatible theranostic nanoplatform based on magnetic gadolinium-chelated polycyclodextrin: *in vitro* and *in vivo* studies. *Carbohydr. Polym.* 2021, *254*, 117262. Epub 2020 Oct 23.
36. Wang X., Sun G., Routh P., Kim D. H., Huang W., Chen P. Heteroatom-doped graphene materials: syntheses, properties and applications. *Chem. Soc. Rev.* 2014, *43*, 7067–7098.
37. Chen L., Zhong X., Yi X., Huang M., Ning P., Liu T., Ge C., Chai Z., Liu Z., Yang K. Radionuclide ^{131}I labeled reduced graphene oxide for nuclear imaging guided combined radio- and photothermal therapy of cancer. *Biomaterials* 2015, *66*, 21–28.
38. Challan S. B., Massoud A. A. Radiolabeling of graphene oxide by Tchnetium-99m for infection imaging in rats. *J. Radioanal. Nucl. Chem*. 2017, *314*, 2189–2199.

39. Yang Y., Magalhães Rebelo Alencar L., Sahylí Ortega Pijeira M., Silva Batista B., Roger Silva França A., Rafael Dias Rates E., Cardoso Lima R., Gemini-Piperni S., Santos-Oliveirac R. [^{223}Ra] $RaCl_2$ nanomicelles showed potent effect against osteosarcoma: targeted alpha therapy in the nanotechnology era. *Drug Deliv.* 2022, *29*, 186–191.
40. Wu X., Dawsey A. C., Siriwardena-Mahanama B. N., Allen M. J., Williams T. J. A (Fluoroalkyl) guanidine modulates the relaxivity of a phosphonate-containing T_1-shortening contrast agent. *J. Fluor. Chem.* 2014, *168*, 177–183.
41. Rohrer M., Bauer H., Mintorovitch J., Requardt M., Weinmann H.-J. Comparison of magnetic properties of MRI contrast media solutions at different magnetic field strengths. *Investig. Radiol.* 2005, *40*, 715–724.
42. Chen F., Bu W., Zhang S., Liu J., Fan W., Zhou L., Peng W., Shi J. Gd^{3+}-ion-doped upconversion nanoprobes: relaxivity mechanism probing and sensitivity optimization. *Adv. Funct. Mater.* 2013, *223*, 298–307.